Composites Science and Technology 151 (2017) 1–9

Contents lists available at ScienceDirect

Composites Science and Technology

journal homepage: http://www.elsevier.com/locate/compscitech

Repeated healing of delamination damage in vascular composites by pressurized delivery of reactive agents

Kevin R. Hart [a, b], Seth M. Lankford [a], Isaac A. Freund [a], Jason F. Patrick [b], Brett. P. Krull [b, c], Eric D. Wetzel [d], Nancy R. Sottos [b, c], Scott R. White [a, b, *]

[a] Department of Aerospace Engineering, University of Illinois at Urbana-Champaign, 104 S. Wright St., Urbana, IL 61801, USA
[b] Beckman Institute for Advanced Science and Technology, University of Illinois at Urbana-Champaign, 405 N. Mathews Ave., Urbana, IL 61801, USA
[c] Department of Materials Science and Engineering, University of Illinois at Urbana-Champaign, 1304 W. Green St., Urbana, IL 61801, USA
[d] U.S. Army Research Laboratory, Composite and Hybrid Materials Branch, Aberdeen Proving Ground, MD 21005, USA

ARTICLE INFO

Article history:
Received 8 February 2017
Received in revised form
10 June 2017
Accepted 26 July 2017
Available online 27 July 2017

Keywords:
Self-healing
Vascular
Fiber-reinforced composites
Raman spectroscopy

ABSTRACT

Recurrent self-healing of fracture damage in fiber-reinforced composites was accomplished by incorporating internal vascular networks for repeated delivery of reactive liquid components to an internal delamination. Double cantilever beam specimens containing embedded microvascular channels were repeatedly fractured and healed by pumping individually sequestered epoxy and amine based healing agents to the fracture plane. The effect of various pumping parameters and component delivery ratios on *in situ* mixing of the healing agents and the resulting healing efficiency is reported. Confocal Raman spectroscopy was used to quantify the extent of mixing of healing agents within the fracture plane. Using an optimized healing agent delivery scheme, ten cycles of fracture and healing were achieved with, on average, 55% and as high as 95%, recovery of the virgin critical strain energy release rate.

1. Introduction

Fiber-reinforced polymer (FRP) composites are now commonplace in the aerospace, automotive, wind energy, marine, and sporting good industries because of their unparalleled specific mechanical properties when compared to traditional engineering materials. However, the matrices of FRP composites are typically made from a brittle thermosetting resin, rendering these structural materials susceptible to crack initiation and growth. In order to combat the flaw sensitivity of FRP composites, many researchers have explored biologically inspired self-healing concepts as an alternative to traditionally expensive repair techniques, including the exploration of internal, bio-mimetic vascular networks for delivery of chemically reactive healing agents to damaged regions of the composite structure [1].

Self-healing microvascular fiber-reinforced composites were first explored using hollow glass fibers (HGFs) for the delivery of reactive liquid components to damaged regions. Bleay et al. investigated the release of pre-mixed liquid epoxy resin from HGFs after impact in quasi-isotropic composites via optical microscopy and x-ray radiography, showing that only partial filling of the damage regions occurred at room temperature conditions, but improved filling occurred at elevated healing temperatures under vacuum [2]. In later studies, Pang and Bond used larger diameter HGFs to investigate a two-part epoxy healing system with components sequestered in separate, orthogonal HGF layers in order to recover flexural strength after indentation damage [3,4]. More recently, Williams et al. demonstrated 100% recovery of compression after impact strength in carbon fiber laminates containing HGFs which were pre-filled with pre-mixed epoxy healing agents and subject to heating immediately after impact [5]. However, in all studies utilizing HGFs the autonomy and repeated healing were severely limited because samples required pre-mixed healing agents, solvent aided dilution/infiltration, heating, and/or vacuum infiltration of healing agents.

Advances in manufacturing have enabled new methods for fabricating vascular composites. Williams et al. constructed self-healing networks within composite sandwich panels using polyvinyl chloride tubes in the core region of the panel that contained the healing agents. Impacted sandwich panels recovered greater than 100% of their virgin strength when healed with pre-mixed

* Corresponding author. Department of Aerospace Engineering, University of Illinois at Urbana-Champaign, 104 S. Wright St., Urbana, IL 61801, USA.
E-mail address: swhite@illinois.edu (S.R. White).
URL: http://www.whitegroup.beckman.illinois.edu

http://dx.doi.org/10.1016/j.compscitech.2017.07.027
0266-3538/

epoxy resin [6]. Norris et al. used elevated temperature evacuation of solder wire or manual extraction of Teflon coated steel wires after composite fabrication to create isolated vascular channels in carbon fiber/epoxy laminates. Pre-mixed epoxy resin was injected into impact damage to demonstrate recovery of mechanical performance for one healing cycle [7–9]. Patrick et al. [10] utilized the Vaporization of Sacrificial Components (VaSC) process introduced by Esser Kahn et al. [11] to fabricate complex internal vascular networks in woven glass/epoxy double cantilever beam (DCB) specimens. Greater than 100% recovery of mode I critical strain energy release rate was obtained over three fracture/healing cycles using pressurized delivery and *in situ* mixing of a segregated two-part epoxy healing agent system. However, subsequent heal cycles predicated crack advancement into virgin material to improve fluid dispersion and *in situ* mixing. More recently, Wang et al. [16] fabricated microvascular composites with porous copper and carbon nanotube interleaves to perform resistive heating assisted healing of DCB specimens in a low temperature (ca. −60 °C) environment. Specimens demonstrated up to 100% healing of critical strain energy release rates, but were limited to a single healing cycle.

Robust and efficient vascular healing requires a network capable of recurrent delivery of individually sequestered healing agents and which promotes adequate *in situ* mixing of the agents. Hamilton et al. fabricated a model system for pressurized delivery of healing agents to recover mode I fracture damage in double cleavage drilled compression bulk epoxy specimens. Individual healing agents were pumped in an alternating fashion to the damage region and authors demonstrated that dynamic pumping schemes enabled up to 15 healing cycles of greater than 90% efficiency [12], an advancement over the authors' previous work using static delivery through a dense ensemble of channels [21]. However, an explicit relationship between the degree of *in situ* mixing of components and the healing efficiency was not presented. We summarize in Table 1 the history and current state-of-art for the self-healing of internal damage using a variety of vascular approaches.

In this work, we employ pressurized delivery of a two-part epoxy/amine healing system through microchannels created within a woven glass/epoxy composite. The vasculature and pulsed pumping schemes are designed to promote *in situ* mixing and polymerization of healing agents. DCB fracture testing is performed while investigating the effect of component delivery ratios and pulsed pumping profiles on healing efficiency. Raman spectroscopy is used to assess the degree of *in situ* mixing of healing agents. The best delivery scheme tested enabled 10 cycles of fracture and healing of a mid-plane delamination crack.

2. Experimental methods

2.1. Double cantilever beam specimen manufacture

To prepare vascularized composites, 4 layers of 814 g/m^2, 2 × 2 tows/cm, S2-glass plain weave fabric (Owens Corning; Toledo, OH) measuring 27.9 × 27.9 cm were arranged in a $[0/90]_s$ sequence. An ethylene tetrafluoroethylene (ETFE) release film (Airtech International Inc.; Hutington Beach, CA) measuring 8.9 × 27.9 cm was then placed in the mid-plane at the edge of the preform to serve as a pre-crack in subsequent fracture testing. Sacrificial fiber monofilaments (500 μm diameter), prepared according to Esser Kahn et al. [11], were then stitched into the 4-layer preform with a center to center spacing of 2 mm, to define the microchannel network. One additional layer of reinforcement was then placed on both the top and bottom layers of the stitched preform to embed the sacrificial fibers within the preform stack, yielding a final lay-up sequence of $[90/0/90]_s$. Araldite LY/Aradure 8605 epoxy resin (100:30 ratio w/w%; Huntsman Mfg.; Alvin, TX) was infused into the preform by vacuum assisted resin transfer molding (VARTM) under vacuum at 36 torr. After 30 h at 23 °C, the solidified composite was removed from vacuum and placed in a convection oven for 2 h at 121 °C and an additional 3 h at 177 °C to complete the manufacturer's recommend cure cycle. After curing and machining to size, samples were placed flat in a vacuum oven at 200 °C for 24 h to evacuate the sacrificial fibers. Previous work by Coppola et al. [20] conclusively demonstrated that the mechanical properties of the host material are unaffected by this heat treatment process. The revealed microchannels were sequentially flushed with acetone, de-ionized water, and air to clear any minor amount of residual sacrificial material.

Double cantilever beam specimens were cut from the cured panel to the dimensions depicted in Fig. 1a using a water cooled diamond saw. The DCB specimen contains three internal microchannels that traverse the entire length of the specimen. A triplet

Table 1
Comparison of results and approaches for self-healing of internal damage using a vascular delivery scheme.

Reference	Year	Host material*	Evaluation metric	Microchannel incorporation	Healing agent incorporation	Healing agent mixing	Pumping scheme	Max number of healing cycles	Max healing efficiency
Bleay et al. [2]	2001	CFRP	Optical	Hollow Glass Fibers	Post-Damage	Ex-situ	Static	1	NA
Pang et al. [3]	2005	CFRP	Flexure	Hollow Glass Fibers	Pre-Damage	In-situ	Static	1	~65%
Pang et al. [4]	2005	CFRP	Flexure	Hollow Glass Fibers	Pre-Damage	In-situ	Static	1	93%
Williams et al. [5]	2009	CFRP	Compression	Hollow Glass Fibers	Pre-Damage	Ex-situ	Static	1	100%
Williams et al. [6]	2007	CFRP Sandwich	Flexure	PVC Tubes	Pre-Damage	Ex-situ	Static	1	100%
Norris et al. [7]	2011	CFRP	Compression	Solder Evacuation	Post-Damage	Ex-situ	Static	1	99%
Norris et al. [8]	2012	CFRP	Compression	PTFE coated Steel Removal	Impact-Triggered	Ex-situ	Static	1	>100%
Norris et al. [9]	2013	CFRP	Compression	PTFE coated Steel Removal	Post-Damage	Ex-situ	Static	1	>100%
Patrick et al. [10]	2014	GFRP	Mode I Fracture	VaSC	Pre-Damage	In-situ	Dynamic	3	>100%
Wang et al. [16]	2016	GFRP	Mode I Fracture	VaSC	Pre-Damage	Ex-situ	Static	1	>100%
Hamilton et al. [12]	2011	Epoxy	Mode I Fracture	Nylon Fiber Removal	Post-Damage	In-situ	Dynamic	15	100%
Hamilton et al. [21]	2010	Epoxy	Mode I Fracture	Fugitive Ink Dissolution	Pre-Damage	In-situ	Static	13	83%

* GFRP: Glass Fiber Reinforced Plastic. CFRP: Carbon Fiber Reinforced Plastic.

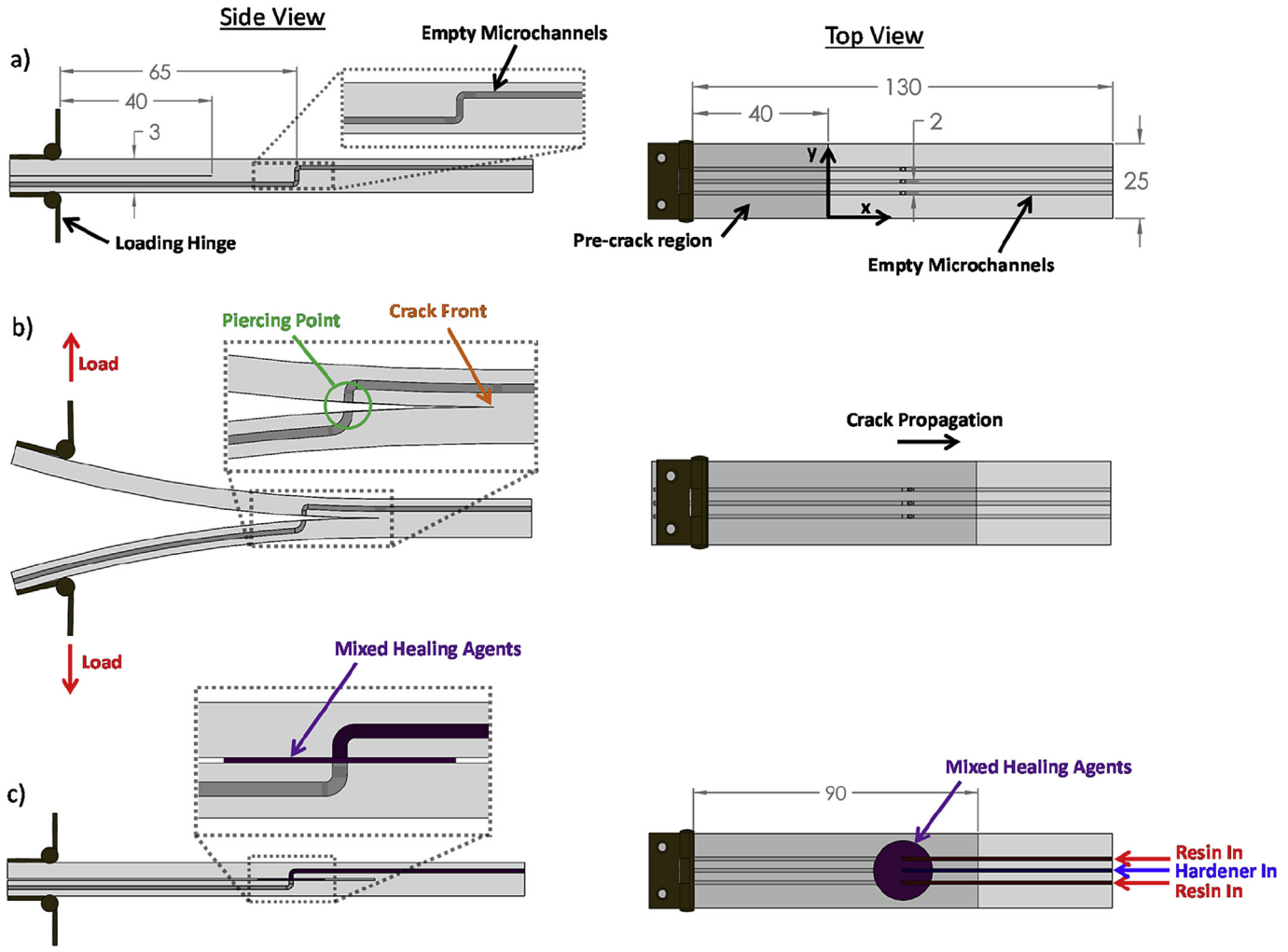

Fig. 1. Microvascular double cantilever beam specimen. (a) Nominal specimen dimensions (in mm). (b) Interlaminar crack propagation opens microchannels to the fracture plane at the piercing point during testing. (c) Subsequent unloading of the specimen followed by pressurization of the microchannels and delivery of the healing agents to the delamination.

channel design was chosen to approximate stoichiometric delivery of healing agents at a volumetric ratio of 2:1. The microchannels are subsequently opened during interlaminar fracture testing after 25 mm of crack propagation at a location designated the 'piercing point' (Fig. 1b). Fracture through the piercing points opens the channels and allows healing agent delivery to the fracture plane. Once the sample is unloaded, the microchannels are pressurized to deliver healing agents to the interlaminar delamination (Fig. 1c). Pressurized delivery of agents did not cause appreciable changes in the sample geometry during infiltration.

2.2. Fracture testing and healing protocols

Mode I fracture testing of DCBs was carried out following ASTM D5528. Samples were loaded at a rate of 250 μm/s and unloaded (where applicable) at 750 μm/s. During the first (virgin) and subsequent (healed) fracture tests, crack propagation was monitored from above the sample using a digital camera (Model A631fc; Basler AG; Ahrensburg, Germany) with a zoom lens (LM16HC; Kowa Optimed Inc.; Torrance, CA) while backlighting the sample during testing and following the optical mismatch induced through crack propagation [13]. In all virgin fracture tests the crack was propagated approximately 50 mm from the pre-crack region then unloaded by returning the crosshead to the initial position of zero displacement. After the sample was unloaded but still in the test frame, liquid epoxy resin EPON 8132 and amine-based hardener Epikure 3046 (Miller-Stephenson; Morton Grove, IL) were delivered through their respective microchannels to the fracture plane using a pressure controlled pump (Ultimus V; EFD Nordson Inc.; East Providence, RI) through 510 μm diameter precision dispense tips (EFD Norton Inc.) following the alternating on/off scheme outlined in Fig. 2. Pump timing and component delivery ratios varied according to the parameters listed in Tables 2 and 3, providing 20 unique pumping profiles that were experimentally evaluated. The range of parameters studied, healing agent selection, and healing conditions utilized were predicated on prior studies using similar epoxy and amine based healing agents [10,12]. Following delivery of healing agents, samples were clamped using two 6.4 mm binder clips at each end of the specimen. The edges of the sample were wiped of excess healing agent and the entire specimen was placed in a 30 °C oven for 48 h to ensure consistent healing conditions. For samples undergoing multiple fracture/healing cycles, microchannels were purged with air (34 kPa) immediately after initial healing agent delivery and maintained throughout the 48 h healing period in order to keep microchannels clear of blockages for subsequent healing cycles [10,17,18]. Without the air purge, delivery channels were occasionally blocked and could not be reused for repeated healing. The vast majority of the

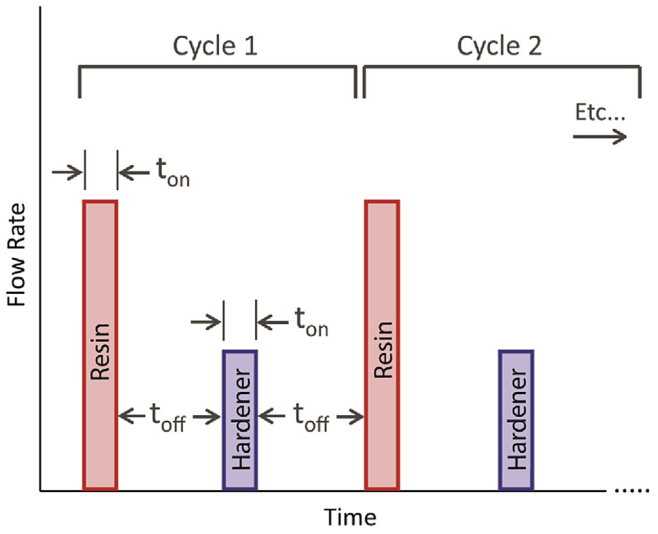

Fig. 2. Dynamic pumping scheme employed for healing agent delivery to the fracture plane. Exact delivery times and flow rates vary as outlined in Table 2.

Table 2
Pressurized pumping profiles for dynamic delivery of self-healing components. One complete cycle includes the individual delivery of the resin and hardener components and the wait time between each component delivery.

Pump timing profiles			
Designation	t_{on} (s)	t_{off} (s)	# Cycles
Short Pulse	3	5	40
Medium Pulse	6	5	20
Long Pulse	12	5	10
Extra Long Pulse	30	10	4

air purge flowed out through the exits of channels, although a small fraction did escape through the crack plane. As a result, liquid healing agents were periodically cleaned from the sample edge during the purge process using a lint-free wipe. Samples subject to only one healing cycle did not experience an air purge during healing. Healed samples were then tested to the same crack propagation length as virgin tests using equivalent loading rates. Samples undergoing multiple healing cycles were unloaded and subject to immediate re-delivery of healing agents and the same healing conditions for up to 10 cycles of crack propagation and healing. Samples used for fracture plane imaging or Raman spectroscopy were completely separated to provide unhindered visual access to the fracture plane after the final healing cycle.

For both virgin and healed fracture tests, critical strain energy release rates were calculated using the area method [10] according to the equation

$$G_{IC} = \frac{\Delta U}{b\Delta a} \tag{1}$$

where G_{IC} is the critical strain energy release rate, b is the sample width, Δa is the change in crack length during testing and ΔU is the change in elastic strain energy, calculated from the area under the load/displacement curves during fracture testing as

$$\Delta U = \left(\int_0^{\delta_f} \left[P(\delta)_{load} - P(\delta)_{unload} \right] d\delta \right) \Bigg|_{\Delta a = 50\ mm} \tag{2}$$

where $P(\delta)_{load}$ and $P(\delta)_{unload}$ are the load and unload curves of the tested sample and δ_f is the displacement at which the crack propagation (Δa) reaches 50 mm and the sample is unloaded. Healing efficiency is then defined as the ratio of virgin to healed critical strain energy release rates as:

$$\eta_i \equiv \frac{G_{IC}^{Healed,i}}{G_{IC}^{Virgin}} \tag{3}$$

where G_{IC}^{Virgin} is the virgin critical strain energy release rate and η_i and $G_{IC}^{Healed,i}$ are the healing efficiency and healed critical strain energy release rate, respectively, of the *ith* healing cycle. Since the virgin and healed specimens have the same width and same final crack length, the definition of healing efficiency simplifies to the ratio of the change in elastic strain energy

$$\eta_i = \frac{\Delta U^{Healed,i}}{\Delta U^{Virgin}}. \tag{4}$$

2.3. Crack plane fractography

Fracture planes of DCB specimens were investigated using fluorescent imaging and electron microscopy to qualitatively characterize the distribution of healing agents on the fracture plane. Fluorescent images were obtained using a digital camera (Model A631fc; Basler AG; Ahrensburg, Germany) with a 50 mm zoom lens (AF Nikkor; Nikon; Chiyoda, Tokoyo, Japan). To enhance fluoresent imaging of the healing agents, EPON 8132 resin was dyed with 0.025 wt% nile red and Epikure 3046 hardener was dyed with 0.050 wt% fluorescein (Sigma Aldrich; St. Louis, MO). Samples were illuminated with 450–465 nm blue LEDs (CREE, Inc.; Durham, NC). Emission of the resin occurred in the visible red spectrum (~625 nm) while the hardener emitted in the green spectrum (~550 nm). The illuminating blue light was filtered by placing a 500 nm longpass optical filter (Edmund Optics; Barrington, NJ) between the illuminated sample and the camera lens. Scanning electron micrographs were obtained on a Quanta 450 FEG-ESEM (FEI Company; Hillsboro, OR) at 10 kV using a secondary electron detector.

Table 3
Component ratios for vascular delivery of self-healing components.

Component delivery ratios				
Designation	Component flow rate per channel, μL/s		Component ratio (R:H, vol.)	Percent resin delivered (v/v%)
	Resin (# channels)	Hardener (# channels)		
Only Resin	1.01 (3)	0 (0)	–	100%
Excess Resin	1.20 (2)	0.63 (1)	1.9: 0.5	79.2%
Stoichiometric	1.00 (2)	1.05 (1)	1.9: 1	65.5%
Excess Hardener	0.74 (2)	1.56 (1)	1.9: 2	48.7%
Only Hardener	0 (0)	1.01 (3)	–	0%

2.4. Raman spectroscopy

Raman spectroscopy has been used previously in the investigation of epoxy-based polymers to determine the degree of cure during the polymerization of epoxy and amine based reactants [10,14,15]. Hardis et al. and Merad et al. both correlated degree of cure calculations using Raman microscopy to the degree of cure calculated using differential scanning calorimetry with good agreement [14,15]. Intensities of the reactive oxirane peak at 1256 cm^{-1} were compared with the reaction invariant phenyl peaks at 1606 cm^{-1} in the epoxy resin to track the degree of cure over time. Patrick et al. similarly monitored the peak oxirane/phenyl ratios during a 48 h cure of various mixtures of EPON 8132 and Epikure 3046 at both room temperature and 30 °C to characterize polymerization [10]. A reaction invariant amide peak at 1649 cm^{-1} was also identified in the amine-based hardener that can be used to quantify the amount of amine present (when compared to other reaction invariant peaks).

In this work, the reaction invariant phenyl and amide peaks in the EPON 8132 epoxy and Epikure 3046 hardener, respectively, were monitored to determine the compositional mix of the healing agents at specific locations along the healed DCB fracture plane. Since both phenyl and amide peaks are reaction invariant, the ratio of the two is also reaction invariant and provides a convenient measure of healing agent composition that is independent of the degree of cure. Stokes Raman spectra were acquired using a Horiba model LabRAM HR 2D Raman confocal imaging microscope with an affixed Andor Newton DU970P EMCCD camera (1600 × 200 pixels) using a 100× objective and a 785 nm near-IR laser. Hardware was controlled and spectra were analyzed with LabSpec 5 (v5.78.24) spectroscopy software. A 950 μm confocal hole diameter, 100 μm slit width, 300 grooves/mm diffraction grating, 60 s acquisition time and a ~1.5 μm spot size diameter on the sample surface were utilized across a spectral range of 1000 cm^{-1} – 2000 cm^{-1}.

2.4.1. Reference calibration

The phenyl to amide peak ratios over a range of concentrations of healing agents were obtained by Raman spectroscopy to provide an *ex-situ* calibration curve. Scintillation vials (20 mL) containing a designated mixture of EPON 8132 and Epikure 3046 were prepared and degassed under vacuum for 15 min. Sample mixtures contained 0%, 29.1%, 45.1%, 52.2%, 62.1%, 68.6%, 76.7%, 86.7%, or 100% EPON 8132 resin by volume, with Epikure 3046 to balance. After degassing, approximately 15 mg of each mixture was placed in an aluminum sample pan and cured in a convection oven at 30 °C for 48 h to simulate healing conditions. Raman spectra were then collected and the ratio of the phenyl to amide peak intensities (Ψ) was recorded as

$$\Psi = \frac{I_{1606cm^{-1}}}{I_{1649cm^{-1}}} \tag{5}$$

where I^{-1}_{1606cm} and I^{-1}_{1649cm} are the Raman spectra intensities at Raman shifts of 1606 cm^{-1} (phenyl moiety) and 1649 cm^{-1} (amide moiety). Example spectra of the EPON 8132 resin and Epikure 3046 hardener, as well as a stoichiometric mixture of the two components after 48 h at 30 °C are provided in Fig. 3. Phenyl to amide peak ratios as a function of resin concentration (v/v%) are provided in Fig. 4. A calibration curve was fit to the data

$$\Psi(R) = c_1\left(\frac{R}{1-R}\right) + c_2, \quad 0 \le R \le 1 \tag{6}$$

where R is the resin concentration (v/v%) in the mixture and c_1 and c_2 are constants from the calibration experiments ($c_1 = 0.774$, $c_2 = 0.323$). Solving for the resin concentration yields

$$R(\Psi) = \frac{\Psi - c_2}{\Psi + (c_1 - c_2)} \tag{7}$$

which allowed for the resin concentration to be determined from the measured phenyl to amide peak ratios at various locations along the fracture planes of healed DCB specimens.

2.4.2. Stoichiometric proximity

With the reference calibration between volumetric resin concentration and phenyl to amide peak ratios established, a metric of stoichiometric proximity was defined as:

$$\theta(R) = \begin{cases} \left[\left(\frac{1}{1.9}\right)\left(\frac{R}{1-R}\right)\right] & , \quad R \le R_s \\ \left[\left(\frac{1}{1.9}\right)\left(\frac{R}{1-R}\right)\right]^{-1} & , \quad R \ge R_s \end{cases} \tag{8}$$

where R is the percentage of EPON 8132 resin (v/v%) in the EPON 8132/Epikure 3046 healing agent mixture, R_s is the volumetric percentage of EPON 8132 for stoichiometric conditions ($R_s = 0.655$), and θ is the stoichiometric proximity. Stoichiometric proximity ranges from zero to one and provides a normalized parameter describing how close the probed material is to stoichiometric conditions; a value of zero indicates either 100% resin (R = 1.0) or 100% hardener (R = 0.0), a value of 0.5 indicates the presence of twice the stoichiometric amount of resin (R = 0.792) or hardener (R = 0.487), and a value of one indicates the presence of healed material at the stoichiometric ratio (R = 0.655).

2.4.3. Assessment of healing agent mixing

Fracture specimens utilized for Raman spectroscopy were probed after one or ten healing cycle(s). Fifteen spatial locations on each fracture plane were investigated across a grid-like sample domain for $x = 5, 15, 25, 35, 45$ mm (fracture propagation direction) and $y = 5, 12.5, 20$ mm (sample width; coordinate axes depicted in Fig. 1a). The stoichiometric proximity, $\theta_{x,y}$, was calculated at each spatial location according to Equation (8). An average stoichiometric proximity ($\bar{\theta}$) was then calculated for each sample across the entire fracture surface. Finally, the average stoichiometric proximity across the width ($\bar{\theta}_y$) was calculated from the resin concentration measured across the range ($y = 5, 12.5$, and 20 mm) at each point along the fracture length ($x = 5, 15, 25, 35, 45$ mm).

3. Results and discussion

3.1. Fracture testing

Representative virgin and healed load-displacement curves from DCB fracture testing are presented in Fig. 5. Both virgin and healed samples display characteristic stick-slip fracture behavior as a result of the coarse fabric architecture of the composite. The average mode I critical strain energy release rate (G_{1C}) of virgin samples was calculated using Equation (1) as 975 ± 88 J/m^2. Previous works have shown that fracture performance of DCBs is unaffected by the presence of the channels if channels are oriented parallel with the crack propagation direction [10,19,22].

3.1.1. Single cycle healing results

Healing efficiency as a function of resin concentration delivered via the pumping protocols described in Section 2.2 is plotted in Fig. 6 for the first healing cycle. The best performance was obtained using a 30 s pulse at the stoichiometric delivery ratio for which 95%

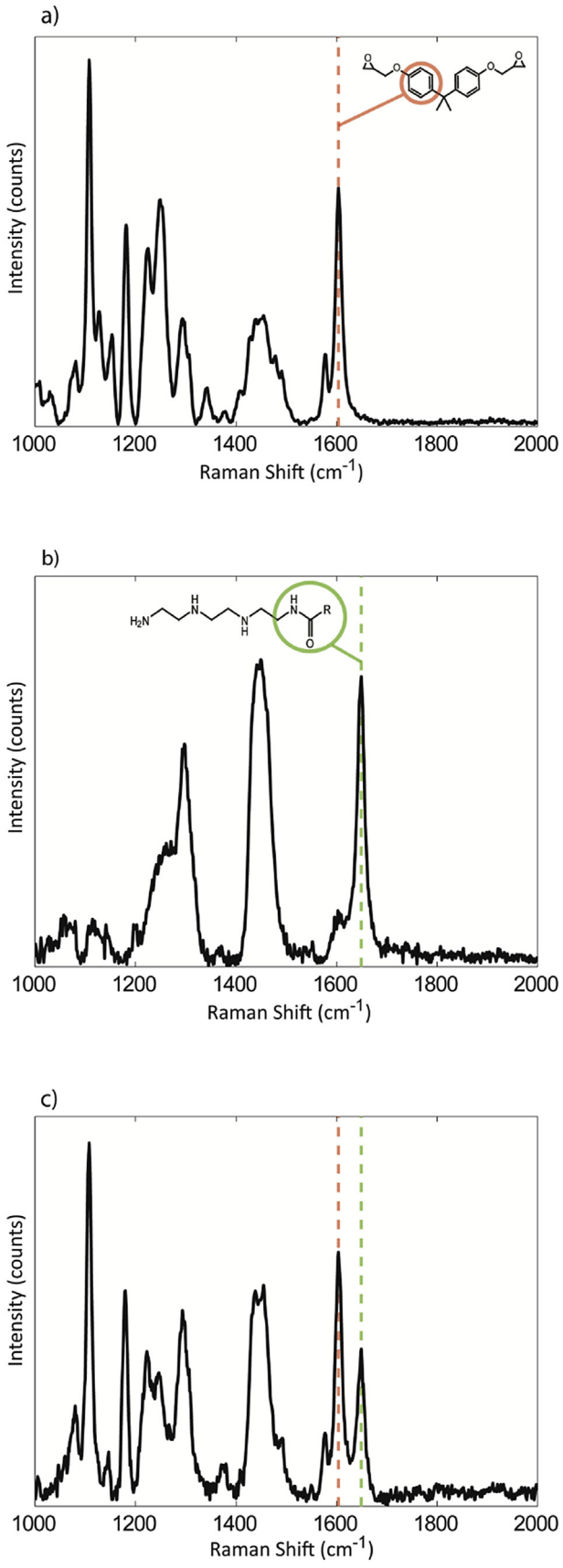

Fig. 3. Raman spectra of healing agents. (a) EPON 8132 epoxy resin. The peak at 1606 cm^{-1} is reaction invariant and a signature of the phenyl moiety of the epoxy monomer molecule. (b) Epikure 3046 hardener. The peak at 1649 cm^{-1} is reaction invariant and a signature of the amide moiety of the hardener molecule. (c) A stoichiometric mixture (R = 0.655) of EPON 8132 and Epikure 3046 after 48 h at 30 °C. The ratio of phenyl (1606 cm^{-1}) to amide (1649 cm^{-1}) peak intensities is used to calculate the *in situ* resin concentration over a particular Raman scan spot size.

of the virgin fracture toughness was recovered. Generally, increased pumping pulse duration led to higher healing efficiency. We hypothesize that improved healing with longer pulse duration is a result of more complete coverage of the crack width between pulses and the resulting better mixing that results from increased folding of healing agents across the entire crack plane [12].

When pumping pulses were long, healing performance was highest when a stoichiometric ratio of healing agents was delivered. Interestingly, healing during the 30 s pulse profile is more tolerant of excess hardener conditions as the healing efficiency was approximately 90% when twice the stoichiometric amount of hardener was delivered. Delivering twice the stoichiometric amount of resin, however, led to lower healing performance, with only 55% recovery measured in the best case. Tolerance of excess hardener, as opposed to excess resin is consistent with previous self-healing studies using vascular delivery [17,18]. In all control samples delivering only resin or hardener components, no healing was observed.

3.1.2. Multiple healing cycles

For all tests involving multiple fracture and healing cycles, healing agents were delivered at stoichiometric conditions with the longest (30 s) pulse since this delivery scheme provided the best performance during single healing cycle testing. Representative load-displacement curves from a sample undergoing multiple fracture and healing cycles are plotted in Fig. 7a. In all cases, a significant drop in load occurred at roughly 20 mm of displacement as the propagating crack reached the piercing point. At this location, agents are not well mixed and the crack rapidly propagated through the sample, evidenced by the large drops in load during fracture testing. Regardless, well-cured material formed approximately 5 mm away from the piercing point and significant recovery of fracture load occurred during the initial loading of the healed specimens. Healing efficiency over ten fracture and healing cycles is plotted in Fig. 7b. Healing performance for all cycles is between $\eta = 0.45$ and 0.67. Testing was terminated after 10 fracture/healing cycles. The recovery of damage over multiple fracture events is a distinct improvement over previous vascular-based composites healing schemes in which only 3 healing cycles were demonstrated [10]. If no blockages develop in the delivery channels, the replenishment of healing agents to the fracture plane can continue indefinitely.

3.2. Fracture plane analysis

A fluorescent image of the fracture surface of a DCB specimen after 10 cycles of healing is shown in Fig. 8a. Colors in the image indicate the presence of the healing agents. Pure resin ($\theta = 0, R = 1$) appears red, pure hardener ($\theta = 0$, $R = 0$) appears green and perfectly mixed components ($\theta = 1$, $R = 0.655$) appears yellow. Green-dominated regions (hardener-rich) are apparent on the left and right margins while red-dominated regions (resin-rich) appear in the center region. Three points of interest designated on the fluorescent image were further investigated by scanning electron microscopy (Fig. 8b). Areas with near stoichiometric conditions ($R \approx 0.655$, Fig. 8b–1) and with excess hardener concentrations ($R < 0.5$, Fig. 8b–2) show hackle marks indicative of fracture through healed material. However, areas of high resin concentration ($R > 0.8$, Fig. 8b–3) have a smooth appearance, indicative of un-polymerized liquid film and poor healing.

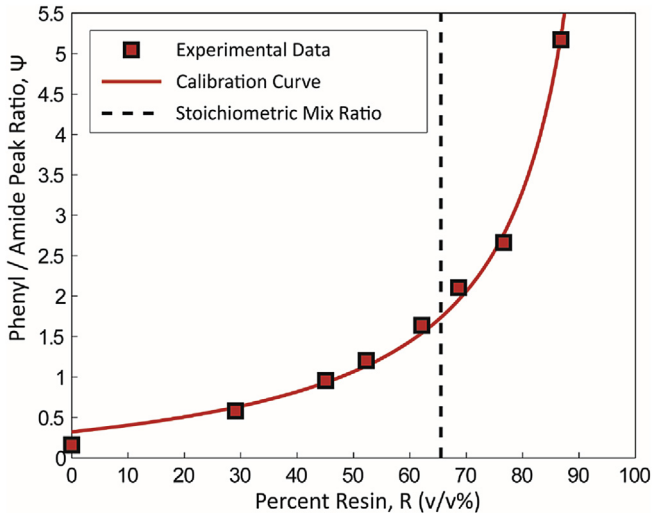

Fig. 4. Calibration of phenyl to amide Raman peak ratios as a function of resin concentration.

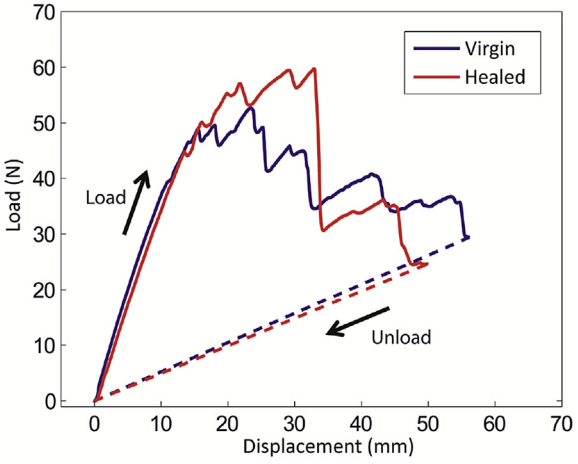

Fig. 5. Representative load-displacement curves from double cantilever beam fracture testing of a virgin and healed sample. Healed data was acquired from a sample subject to the 30 s pulse delivery pumping at a stoichiometric delivery ratio.

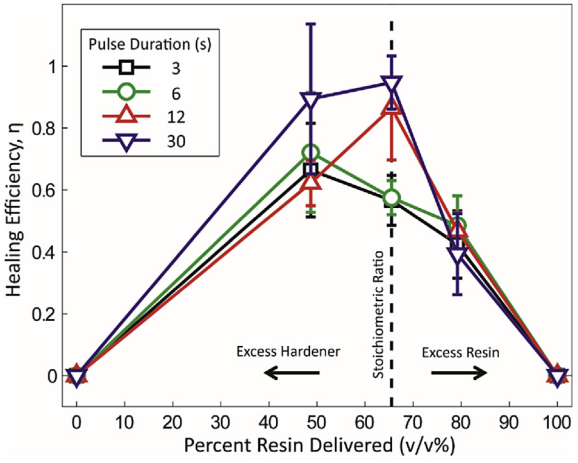

Fig. 6. Healing efficiency (η) as a function of resin concentration delivered for DCB fracture testing. Error bars represent one standard deviation of at least 3 samples for each data point.

3.3. Mixing analysis

The average stoichiometric proximity across the width ($\bar{\theta}_y$) as a function of crack propagation length in a sample subjected to 10 repeat fracture and healing events is plotted in Fig. 9. Stoichiometric proximity is lowest in the vicinity of the piercing point and, as a result, the healing performance in this region is poor. There are two factors contributing to this reduction in performance. Firstly, there is a lack of interfacial folding of the healing agents near the point of delivery, similar to previous healing studies [10]. Secondly, the air purge between mixing cycles forces unreacted healing agents (near the piercing point) out of the crack plane, lowering the healing efficiency.

Finally, in Fig. 10, the average stoichiometric proximity across the entire fracture surface after 10 healing cycles ($\bar{\theta}$) is cross-correlated with the resin concentration delivered. Interestingly, healing efficiencies were high ($\eta = 0.85–0.95$) even with off stoichiometric conditions on the fracture surface ($\bar{\theta} = 0.5–0.6$) indicating that stoichiometric mixing of the components across the entire fracture plane is not required for considerable healing ($\eta > 0.85$) of delamination damage. Stoichiometric proximity and healing efficiency are strongly correlated, confirming that healing performance is directly related to the *in situ* mixing of the healing agents.

3.4. Discussion

For multicomponent healing agents (e.g. 2-part epoxies) the degree of mixing dictates the efficiency of healing as clearly demonstrated by the data in Fig. 10. And yet, Raman data taken from the fracture plane of specimens after healing and re-fracture reveal that mixing is non-uniform across the length (and width) of the central delamination crack (see Fig. 8). Nevertheless, these specimens recover between 50 and 70% of the initial critical strain energy release rate on a repeated basis (Fig. 7). While the work of Hamilton et al. [21] achieved higher healing efficiencies (ca. 90%), the healing protocol required external clamping of the fracture plane closed in this case. In addition, we find that purging the vascular channels with a modest amount of air effectively clears the channels of healing agents and ensures that the channels remain unblocked for subsequent healing cycles. Channel blockage has long been a technological challenge for vascular healing [12,17,21,23] and we believe the air purge approach could be employed in other healing systems as well.

In situ healing of internal delamination damage is critically important because this type of damage represents the most significant threat to composite material health and is often the most difficult to detect [24]. The specimen design and the healing protocol employed here exhibit prolonged and effective recovery of fracture resistance in response to repetitive delamination. While the procedure is not fully autonomous, it could prove effective and practical for high value and critical applications where the added cost and complexity of assisted repair is warranted. Both depot or “in field” repair would simply require connection of the vascular network within the structural component to an external pumping system. After the injection and purge cycle, healing would commence without further human interaction.

4. Conclusions

Healing of delamination damage was achieved in vascular glass/epoxy composite double cantilever beam specimens by delivery of two-part healing agents through internal microchannels. This work demonstrates for the first time that repetitive healing of delamination damage in fiber-reinforced composites can be achieved over

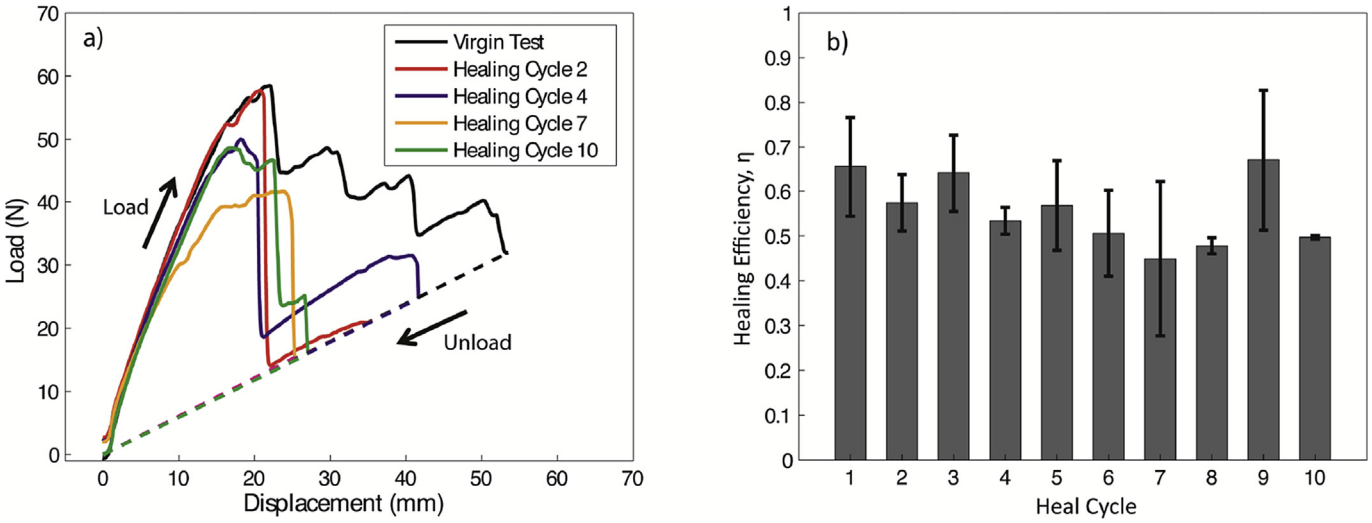

Fig. 7. Repeated fracture and healing cycles for a 30 s pulse pumping profile and stoichiometric healing agent delivery ratio. (a) Representative load-displacement curves for a single DCB sample undergoing multiple fracture/healing cycles. (b) Healing efficiency as a function of healing cycle. Error bars represent one standard deviation of the healing efficiency calculations from three samples.

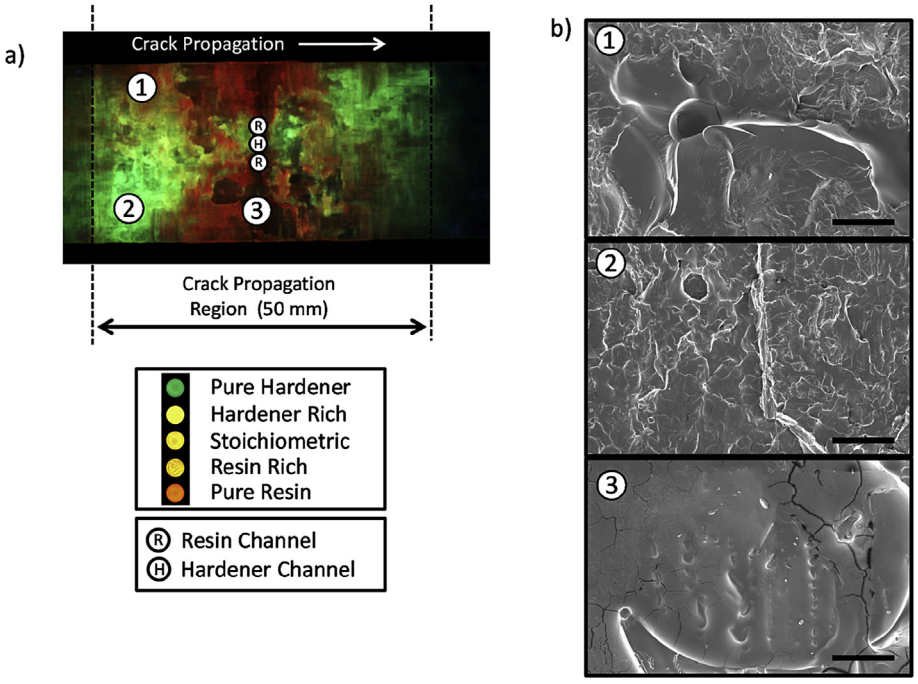

Fig. 8. DCB fracture plane analysis after 10 fracture/healing cycles, for a 30 s pulse duration profile and stoichiometric delivery ratio. (a) Fluorescent imaging of the healed fracture plane. Resin was dyed with 0.025 wt% nile red, fluorescing in the visible red spectra (~625 nm). Hardener was dyed with 0.050 wt% fluorescein, fluorescing in the visible green spectra (~550 nm). (b) Scanning electron microscope micrographs of locations designated (1–3) on (a). Notes: Fracture propagation is left to right in all images. All scale bars are 400 μm. (For interpretation of the references to colour in this figure legend, the reader is referred to the web version of this article.)

multiple (ca. 10) cycles through the use of a pressurized delivery scheme coupled with purge cycles to maintain channel clearance. A variety of dynamic pumping protocols were investigated and the best recovery performance was achieved using a simple on/off pumping scheme with 30 s pumping pulse durations that deliver sufficient volume of healing agents to cover the entire width of the crack plane, promoting increased folding of healing agent interfaces and improved mixing. Delivery of components at stoichiometric conditions provided the best healing performance, but healing efficiencies were still high (>85%) when excess amine-based hardener (double the stoichiometric amount) was delivered. Excess resin delivery was less effective as efficiencies only reached ca. 50% across all pumping protocols investigated. Samples subject to multiple healing cycles showed lower healing efficiencies (ca. 60%) as a result of the air purge used to keep channels clear of blockages. However, 10 healing cycles were repeated with up to 67% healing efficiency throughout. We define a new parameter called *stoichiometric proximity* to characterize mixing efficiency in the fracture plane based on characteristic Raman peaks of the epoxy healing agent system employed. Stoichiometric proximity was shown to

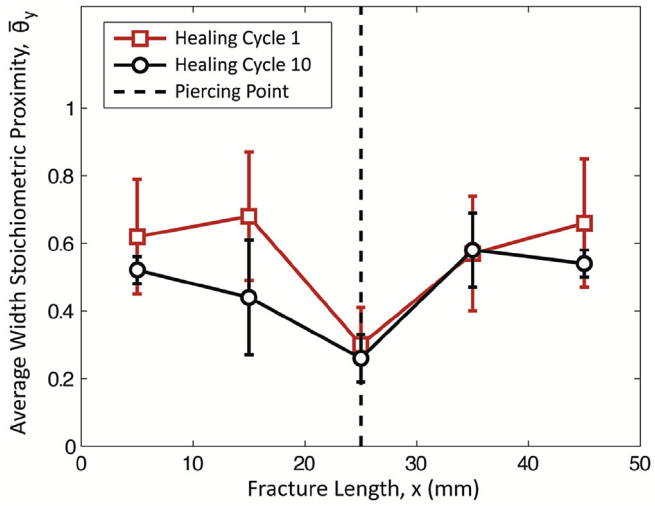

Fig. 9. The average width stoichiometric proximity as a function of length along the fracture plane for 1 or 10 cycle(s) of fracture and healing. Error bars represent one standard deviation.

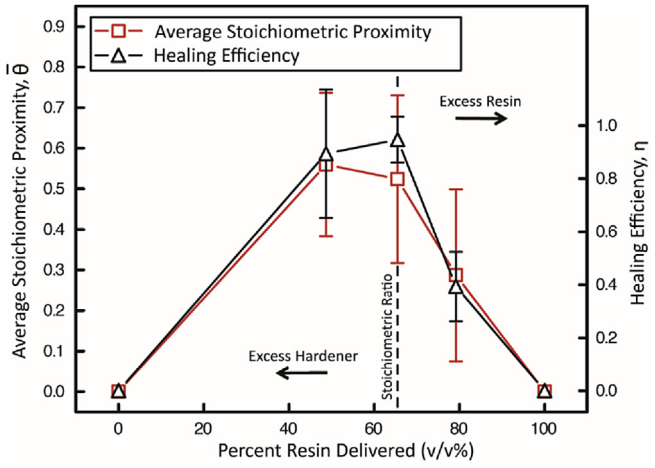

Fig. 10. Average stoichiometric proximity ($\bar{\theta}$) and healing efficiency (η) as a function of percent resin delivered for double cantilever beam specimens utilizing the 30 s pulse pumping profile after 10 cycles. Error bars of the average stoichiometric proximity represent the standard deviation of fifteen values measured across a single sample's healed fracture surface. Error bars of the healing efficiency represent the standard deviation from three fracture samples.

directly correlate with healing efficiency. Thus, the quality of healing provided by vascular delivery of reactive components is directly dependent on the degree and quality of (*in situ*) mixing of the healing agent components in the crack plane.

Acknowledgements

The authors gratefully acknowledge Mr. Gregory Milner, Mr. Steve Mathine, and Mr. Lee Booher for assistance with sample fabrication, as well as Dr. Scott Robinson, Dr. Dianwen Zhang, and Dr. Travis Ross of the Imaging Technology Group at the Beckman Institute for assistance with Raman spectroscopy and image processing. Funding for this work was provided, in part, by the U.S. Army Research Laboratory (grant number W911NF-14-2-003).

References

[1] B.J. Blaiszik, S.L.B. Kramer, S.C. Olugebefola, J.S. Moore, N.R. Sottos, S.R. White, Self-healing polymers and composites, Annu. Rev. Mater. Res. 40 (1) (Jun. 2010) 179–211.
[2] S. Bleay, C. Loader, V. Hawyes, L. Humberstone, P. Curtis, A smart repair system for polymer matrix composites, Compos. Part A Appl. Sci. Manuf. 32 (12) (Dec. 2001) 1767–1776.
[3] J.W.C. Pang, I.P. Bond, 'Bleeding composites'—damage detection and self-repair using a biomimetic approach, Compos. Part A Appl. Sci. Manuf. 36 (2) (Feb. 2005) 183–188.
[4] J.W.C. Pang, I.P. Bond, A hollow fibre reinforced polymer composite encompassing self-healing and enhanced damage visibility, Compos. Sci. Technol. 65 (11–12) (Sep. 2005) 1791–1799.
[5] G.J. Williams, I.P. Bond, R.S. Trask, Compression after impact assessment of self-healing CFRP, Compos. Part A Appl. Sci. Manuf. 40 (9) (Sep. 2009) 1399–1406.
[6] H.R. Williams, R.S. Trask, I.P. Bond, Self-healing sandwich panels: restoration of compressive strength after impact, Compos. Sci. Technol. 68 (15–16) (Dec. 2008) 3171–3177.
[7] C.J. Norris, G.J. Meadway, M.J. O'Sullivan, I.P. Bond, R.S. Trask, Self-healing fibre reinforced composites via a bioinspired vasculature, Adv. Funct. Mater. 21 (19) (Oct. 2011) 3624–3633.
[8] C.J. Norris, J.A.P. White, G. McCombe, P. Chatterjee, I.P. Bond, R.S. Trask, Autonomous stimulus triggered self-healing in smart structural composites, Smart Mater. Struct. 21 (9) (Sep. 2012).
[9] C.J. Norris, I.P. Bond, R.S. Trask, Healing of low-velocity impact damage in vascularised composites, Compos. Part A Appl. Sci. Manuf. 44 (Jan. 2013) 78–85.
[10] J.F. Patrick, K.R. Hart, B.P. Krull, C.E. Diesendruck, J.S. Moore, S.R. White, N.R. Sottos, Continuous self-healing life cycle in vascularized structural composites, Adv. Mater. 26 (25) (Jul. 2014) 4302–4308.
[11] A.P. Esser-Kahn, P.R. Thakre, H. Dong, J.F. Patrick, V.K. Vlasko-Vlasov, N.R. Sottos, J.S. Moore, S.R. White, Three-dimensional microvascular fiber-reinforced composites, Adv. Mater. 23 (32) (Aug. 2011) 3654–3658.
[12] A.R. Hamilton, N.R. Sottos, S.R. White, Pressurized vascular systems for self-healing materials, J. R. Soc. Interface 9 (70) (May 2012) 1020–1028.
[13] B. Krull, J. Patrick, K. Hart, S. White, N. Sottos, Automatic optical crack tracking for double cantilever beam specimens, Exp. Tech. 40 (Jun. 2016) 937–945.
[14] R. Hardis, J.L.P. Jessop, F.E. Peters, M.R. Kessler, Cure kinetics characterization and monitoring of an epoxy resin using DSC, Raman spectroscopy, and DEA, Compos. Part A Appl. Sci. Manuf. 49 (Jun. 2013) 100–108.
[15] L. Merad, M. Cochez, S. Margueron, F. Jauchem, M. Ferriol, B. Benyoucef, P. Bourson, In-situ monitoring of the curing of epoxy resins by Raman spectroscopy, Polym. Test. 28 (1) (Feb. 2009) 42–45.
[16] Y. Wang, D.T. Phan, Z. Zhang, J. Li, C. Ji, Y. Liu, J. Leng, Sustainable self-healing at ultra-low temperatures in structural composites incorporating hollow vessels and heating elements, R. Soc. Open Sci. 3 (Sept. 2016), http://dx.doi.org/10.1098/rsos160488, 160488.
[17] K.S. Toohey, C.J. Hansen, J.A. Lewis, S.R. White, N.R. Sottos, Delivery of two-Part Self-healing chemistry via microvascular networks, Adv. Funct. Mater. 19 (Mar. 2009) 1399.
[18] C.J. Hansen, S.R. White, N.R. Sottos, J.A. Lewis, Accelerated self-healing via ternary interpenetrating microvascular networks, Adv. Funct. Mater. 21 (Sept. 2011) 4320.
[19] C.J. Norris, I.P. Bond, R.R. Trask, Interactions between propagating cracks and bioinspired self-healing vascules embedded in glass fibre reinforced composites, Compos. Sci. Technol. 12 (April 2011) 847–853.
[20] A.M. Coppola, P.R. Thakre, N.R. Sottos, S.R. White, Tensile properties and damage evolution in vascular 3D woven glass/epoxy composites, Compos. Part A Appl. Sci. Manuf. 59 (1) (Dec. 2013) 9–17.
[21] A.R. Hamilton, N.R. Sottos, S.R. White, Self-healing of internal damage in synthetic vascular materials, Adv. Mater 22 (45) (Dec. 2010) 5159–5163.
[22] T. Yang, C.H. Wang, J. Zhang, S. He, A.P. Mouritz, Toughening and self-healing of epoxy matrix laminates using mendable polymer stitching, Compos. Sci. Technol. 72 (12) (Jul. 2012) 1396–1401.
[23] C.J. Hansen, W. Wu, K.S. Toohey, N.R. Sottos, S.R. White, J.A. Lewis, Self-healing materials with interpenetrating microvascular networks, Adv. Mater. 21 (2009) 4143–4147.
[24] W.J. Cantwell, J. Morton, The impact resistance of composite materials — a review, Composites 22 (5) (Sep. 1991) 347–362.